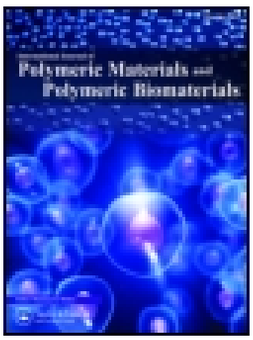

International Journal of Polymeric Materials and Polymeric Biomaterials

ISSN: 0091-4037 (Print) 1563-535X (Online) Journal homepage: https://www.tandfonline.com/loi/gpom20

Influence of chitosan-tripolyphosphate nanoparticles on thermosensitive polymeric hydrogels: structural organization, drug release mechanisms and cytotoxicity

Kelli C. Freitas Mariano, Mônica H. Monteiro do Nascimento, Samyr M. Querobino, Estefânia V. Ramos Campos, Jhones L. de Oliveira, Fabiano Yokaichiya, Margareth K.K.D. Franco, Carlos Alberto-Silva, Eneida de Paula, Christiane B. Lombello, Renata de Lima, Leonardo F. Fraceto & Daniele R. de Araujo

To cite this article: Kelli C. Freitas Mariano, Mônica H. Monteiro do Nascimento, Samyr M. Querobino, Estefânia V. Ramos Campos, Jhones L. de Oliveira, Fabiano Yokaichiya, Margareth K.K.D. Franco, Carlos Alberto-Silva, Eneida de Paula, Christiane B. Lombello, Renata de Lima, Leonardo F. Fraceto & Daniele R. de Araujo (2019): Influence of chitosan-tripolyphosphate nanoparticles on thermosensitive polymeric hydrogels: structural organization, drug release mechanisms and cytotoxicity, International Journal of Polymeric Materials and Polymeric Biomaterials, DOI: 10.1080/00914037.2019.1596909

To link to this article: https://doi.org/10.1080/00914037.2019.1596909

View supplementary material

Published online: 12 Apr 2019.

Submit your article to this journal

Article views: 99

View related articles

View Crossmark data

Full Terms & Conditions of access and use can be found at
https://www.tandfonline.com/action/journalInformation?journalCode=gpom20

INTERNATIONAL JOURNAL OF POLYMERIC MATERIALS AND POLYMERIC BIOMATERIALS
https://doi.org/10.1080/00914037.2019.1596909

Taylor & Francis
Taylor & Francis Group

Check for updates

Influence of chitosan-tripolyphosphate nanoparticles on thermosensitive polymeric hydrogels: structural organization, drug release mechanisms and cytotoxicity

Kelli C. Freitas Mariano[a], Mônica H. Monteiro do Nascimento[a], Samyr M. Querobino[a], Estefânia V. Ramos Campos[b], Jhones L. de Oliveira[b], Fabiano Yokaichiya[c], Margareth K.K.D. Franco[d], Carlos Alberto-Silva[a], Eneida de Paula[e], Christiane B. Lombello[f], Renata de Lima[g], Leonardo F. Fraceto[b], and Daniele R. de Araujo[a]

[a]Human and Natural Sciences Center, Federal University of ABC, Santo André, SP, Brazil; [b]Department of Environmental Engineering, State University "Júlio de Mesquita Filho", Sorocaba, SP, Brazil; [c]Department Quantum Phenomena in Novel Materials, Helmholtz-Zentrum Berlin für Materialien, Berlin, Germany; [d]Nuclear and Energy Research Institute, São Paulo, SP, Brazil; [e]Department of Biochemistry and Tissue Biology, Institute of Biology, University of Campinas, Campinas, São Paulo, Brazil; [f]Engineering, Modelling and Applied Social Sciences Center, Federal University of ABC, Santo André, SP, Brazil; [g]Department of Biotechnology, University of Sorocaba, Sorocaba, Brazil

ABSTRACT

Chitosan-tripolyphosphate (CS-TPP) nanoparticles containing naproxen (NPX) were dispersed in poloxamer (PL) as unique (PL407) or binary (PL407-PL403) systems. Nanoparticles presented diameter of ~250 nm and zeta potential of ~35 mV with drug loading and encapsulation efficiency of 98.4 ± 0.3% and 36.9 ± 0.12%, respectively. NPX-CS-TPP shifted the sol-gel transition and micellization temperatures. PL407-PL403 systems presented $G' > G''$ compared to PL407. SAXS patterns revealed transitions from lamellar to hexagonal phase organizations with low drug release rates, in the presence of CS-TPP nanoparticles. NPX-CS-TPP-PL407 induced lower cytotoxicity compared to PL407-PL403 in fibroblasts and osteoblasts, making them promising systems for intra-articular delivery.

GRAPHICAL ABSTRACT

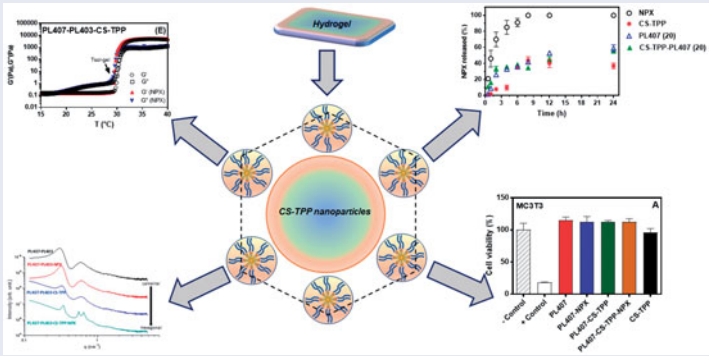

ARTICLE HISTORY
Received 16 November 2018
Accepted 14 March 2019

KEYWORDS
Arthritis; chitosan nanoparticles; hydrogels; naproxen; poloxamer

1. Introduction

Rheumatoid arthritis (RA) is a chronic inflammatory process characterized by the degeneration of cartilage and bone, and the clinical signs include pain, redness, increased local temperature, and swelling in the affected joints. These symptoms are the result of the infiltration of neutrophils, T and B lymphocytes, and macrophages combined with the local release of extracellular matrix metalloproteinases, cytokines, and reactive oxygen species. These mediators induce the inhibition of proteoglycan synthesis, resulting in cartilage degeneration, progressive erosion, and bone loss[1,2].

Naproxen (NPX) is a non-steroidal anti-inflammatory drug (NSAID) that inhibits the activity of COX_1 and COX_2 enzymes, thus reducing the biosynthesis and release of prostaglandins and other inflammation mediators[3]. As a single therapy or in pharmacotherapeutic combinations, the therapeutic effects of NPX lead to the recovery of subchondral bone lesions[4]. However, the oral administration of NPX

CONTACT Dr. Daniele Ribeiro de Araujo daniele.araujo@ufabc.edu.br, draraujo2008@gmail.com Human and Natural Sciences Center, Centro de Ciências Naturais e Humanas, Universidade Federal do ABC, UFABC. Av. dos Estados 5001, Bloco A, Torre 3, Lab 503-3, Bairro Bangú. Santo André, SP, Brasil. CEP 090210-580.

Color versions of one or more of the figures in the article can be found online at www.tandfonline.com/gpom.

Supplemental data for this article can be accessed on the publisher's website.

© 2019 Taylor & Francis Group, LLC

can have significant adverse effects, such as toxicity to the gastrointestinal tract. Thus, in order to reduce the systemic side effects, alternative routes of administration have been proposed, such as topical application[5–7] and especially intra-articular injection[8–10]. The goal is to maintain clinically effective concentrations and increase drug residence in the synovial space.

Different carriers systems have been studied for NPX intra-articular delivery, such as PLGA microspheres[11] and oily depot formulations (medium-chain triglycerides and castor oil)[12–14], which show an increase of the drug residence time in synovial fluid. Similar results have also been presented using dextran polymeric nanoparticles[13]. The development of new formulations for NPX release could make it possible to reduce the number of injections and thus promote patient compliance.

We propose the use of chitosan (CS) nanoparticles cross-linked with tripolyphosphate (TPP) for NPX encapsulation, which have low cost, high biocompatibility, low toxicity, and biodegradability. Additionally, few reports indicate that CS-TPP is an attractive system for intra-articular drug-delivery[14–17]. However, the low viscosity of this system could reduce the retention of the drug in the joints. Therefore, the use of a thermosensitive hydrogel matrix such as poloxamer (PL) would be of great interest for improving the rheological properties and increasing the drug residence in the synovial space. *In fact, polymeric micellar systems have been used as drug delivery matrices for several purposes including anti-cancer*[18–21]*; cardiovascular, Parkinson's disease*[22] *and gene delivery*[23]. However, specifically for arthritis treatment, a recent study reported the development of CS-clodronate nanoparticles loaded in PL gel and showed more pronounced therapeutic effects compared to the free clodronate[15].

In this study, the incorporation of CS-TPP nanoparticles in single or binary PL hydrogels with different hydrophilic-lipophilic balance (HLB) values (PL407: PEO_{100}-PPO_{70}-PEO_{100}, HLB = 22; PL403: PEO_{39}-PPO_{69}-PEO_{39}, HLB = 8) was studied considering the formation of a dual release system with different thermoreversible properties, sol-gel transition and rheological properties. We studied the drug nanoparticles, micelles, and their interaction in the micellization process by light scattering and differential scanning calorimetry (DSC). Small-angle-X-ray scattering (SAXS) was used to study the effects of CS-TPP nanoparticles incorporation on release kinetics and hydrogel supramolecular structure. We also evaluated the cytotoxic effects for use of the hydrogel formulation as possible formulation for intra-articular injection.

2. Materials and Methods

2.1. Synthesis and characterization of chitosan-tripolyphosphate nanoparticles (CS-TPP)

CS-TPP nanoparticles were prepared according to the method described by Grillo et al.[24]. First, 0.1% CS solution (Sigma Aldrich Chem Co., molecular weight: 27 kDa, deacetylation degree of 85%) in 0.2% acetic acid (Ph = 4.7) was prepared under magnetic stirring for 12 h. Next, 0.1% TPP solution was prepared under cooling at 4 °C. Both solutions were filtered through a 0.45-µm filter, and then 5 mL of TPP was added to 20 mL of CS solution and maintained under magnetic stirring for 10 min. The CS-TPP nanoparticles were stored at 25 °C until use.

CS-TPP nanoparticles were characterized by dynamic light scattering (hydrodynamic diameter, size distribution, and polydispersion index) and the zeta potential (NanoSeries ZS90, Malvern® Instruments) before and after NPX incorporation with a total concentration in the formulation of 15 µg.mL^{-1}. The encapsulation efficiency was determined by an ultrafiltration method using a microtube containing a 10-kDa cellulose membrane (Microcon-Millipore) under centrifugation (13,000 × g). The amount of non-encapsulated NPX was quantified in the filtrate by HPLC. The encapsulation efficiency percentage (EE%) and drug loading (DL%) were determined using the following equations:

$$EE\ (\%) = \frac{Drug\ total - Drug\ free}{Drug\ total}\ x\ 100 \quad (1)$$

$$DL\ (\%) = \frac{Drug\ encapsulated\ mass}{Polymer\ mass}\ x\ 100 \quad (2)$$

2.2. Evaluation NPX solubility limit on PL407 and PL407-PL403 solutions

Different solutions (0.5 a 10% m/v) composed of isolated PL407 or in association with PL403 were prepared with excess NPX (2.5 mg.mL^{-1} or 10.9 mM). The dispersions were homogenized and stored for 24 h at 25 °C. The samples were then centrifuged (13,000 × g for 15 min). Aliquots (200 µL) from the supernatant were filtered (0.22-µm pores) and diluted in a solution with a ratio of ethanol to water of 70:30 v/v. The NPX concentration was determined by HPLC.

2.3. Chromatographic conditions for NPX analysis

NPX chromatographic analysis was performed using a UPLC system (UltiMate® 3000, Thermo Sci.) with a quaternary pump (LPG-3400RS), diode array detector (DAD-3000RS), C18 ODS Hypersil column (150 mm × 4.6 mm, 5 µm, Phenomenex® at 25 °C), and mobile phase solution composed of methanol (70%, v/v) and 0.1% acetic acid (30%, v/v). The analysis was conducted with detection at 254 nm, a flow rate of 0.5 mL.min^{-1}, and injection volume of 10 µL. The analytical curve ranged from 1.25 to 20 µg.mL^{-1}, and the analysis presented the following parameters: $y = 0.20447 + 0.94187\ x$; $R^2 = 0.99992$; limit of quantification = 1.19 µg.mL^{-1}; limit of detection = 0.39 µg.mL^{-1}. The retention time was 7.5 min.

2.4. Micellar hydrodynamic diameter

To simulate dilution conditions in physiological medium and to study the drug-micelle or nanoparticle-micelle interaction, a particle analyzer Zetasizer ZS (Malvern®, UK) was

used to determine the micellar hydrodynamic diameter, the average size, and the size distribution at an angle of 173° and temperatures of 25° and 37 °C. After preparation and filtering through a polycarbonate membrane with 0.22-µm pores, solutions of isolated PL 407 or in association with PL 403 (5% m/v in water) were analyzed in the presence or absence of CS-TPP nanoparticles, NPX, or NPX-CS-TPP nanoparticles ($n = 5$/sample).

2.5. CS-TPP nanoparticles in poloxamer hydrogels preparation and physico-chemical characterization

Hydrogels containing CS-TPP nanoparticles were prepared by dispersion at 0.1% v/v relative to the final volume of hydrogel in solutions of 18 or 20% (m/v) isolated PL407 or in binary systems containing 2% PL403 (m/v). They were then maintained at 4 °C under stirring (100 rpm) until the total dissolution of the polymer and dispersion of the nanoparticles. After preparation, the samples were stored at 4 °C until further use. The final concentration of NPX incorporated in the hydrogel system was 1 mg.mL^{-1}. The prepared formulations were named as follows: F1 (18% PL407), F2 (20% PL407), F3 (18% PL407 and 2% PL403), and their respective combinations with NPX, nanoparticles (CS-TPP), and nanoparticles and NPX together (CS-TPP-NPX).

2.6. Differential scanning calorimetry (DSC) analysis

DSC analysis was performed by weighing 20 mg of each sample and sealing them in aluminum pans. The samples were analyzed using a Q-200 DSC device (TA Instruments, USA) with three thermal cycles of heat-cool-heat from 0 °C to 50 °C at a rate of 5 °C/min. An empty pan was used as a reference. Thermograms were obtained in triplicate, and the results are presented as the heat flux (k.J.mol^{-1}) versus temperature (°C).

2.7. Rheological analysis

Rheological analysis was performed using a Kinexus rotational rheometer (Malvern Instruments Ltd., England, UK) with a cone-plate geometry (40 mm in diameter). First, 1 mL of the sample was placed on the plate platform, and measurements were performed in a temperature range of 10–50 °C. An experiment was then carried out at a frequency of 1 Hz and shear stress of 2 Pa to obtain the rheological parameters related to the elastic modulus (G′), viscous modulus (G″), and viscosity (η). Rheograms were obtained using rSpace for Kinexus® software.

2.8. Small Angle X-Ray Scattering (SAXS) experiments

SAXS experiments were carried out using an incident beam energy of 8.3 keV (lambda = 1.488 Å). The distance between the sample and detector was 1007 mm (MarCCD detector with a diameter of 165 mm), and the measurement range (brand measurement range) was 0:13–3:34 nm^{-1} at 37 °C. The measured scattered intensity is displayed as a function of the scattering vector modulus $q = 4\pi\sin(\theta)/\lambda$. The scattering angle is 2θ, and λ is the radiation wavelength. The typical q range was 0.075–0.23 Å^{-1}. The SAXS measurements were carried out at the SAXS 1 beamline (National Laboratory of Synchrotron Light-LNLS, Campinas, SP, Brazil) at two different temperatures (25 and 37 °C).

2.9. In *vitro* release studies

In vitro release assays were carried out in vertical-diffusion Franz-type cells (1.76-cm^2 area, Microette Plus® Hanson Research, CA, USA) with an artificial membrane as a barrier (cellulose acetate sheets, MWCO 1000 Da., Spectrum Lab). The donor compartment was filled with 1 g of each hydrogel, and the receptor compartment was filled with 5 mM Hepes and 154 mM NaCl buffer at pH 7.4 and 37 °C, which was maintained under constant magnetic stirring (350 rpm). Aliquots from the receptor compartment were withdrawn (1 mL) and analyzed by HPLC at determined intervals (0.5, 1, 2, 4, 8, 12, and 24 h). Data were expressed as the percentage of NPX released for each sample ($n = 6$).

The *in vitro* release data were analyzed using the following mathematical models:

$$Qt = Q_0 + K_0.t \quad (3)$$

where Qt is the cumulative amount of drug released at time t, Q_0 is the initial amount of drug, K_0 the zero-order release constant, and t is time.

$$Qt = K_H.t_{1/2} \quad (4)$$

K_H is the release coefficient, which follows Fick's law, and Qt is the amount of drug released.

$$Mt/M\infty = K_{KP}.t^n \quad (5)$$

$Mt/M\infty$ is the fraction of drug released at time t, K_{KP} is the release constant, and n is the release exponent. An n value of 0.45 represents Fickian diffusion, $0.45 < n < 0.89$ indicates anomalous (non-Fickian) diffusion, $n = 0.89$ indicates case-II transport, and $n > 0.89$ indicates super case-II transport.

2.10. In vitro *cytotoxicity assays*

Cytotoxicity assays were carried out according to the ISO 10993-5 recommendations using two cell lines: MC3T3 pre-ostheoblasts and VERO kidney epithelial cells. Cells were seeded in 96-well plates and cultured for 48 h (1.10^4 cells/well) in a specific medium (Ham F-10 and DMEM for MC3T3 and VERO cells, respectively) supplemented with 10% fetal bovine serum (pH 7.2–7.4, humidified atmosphere at 37 °C and 5% CO_2), and 100 µg.mL^{-1} of penicillin/streptomycin cells.

Before cell treatment, the hydrogel formulations were sterilized by autoclaving at 121 °C for 15 min[25], and aliquots of 1 mL were diluted in 4 mL of cell culture medium (5% m/v, PL final concentration). The cells were then incubated for 24 h with NPX, PL 407, PL407-PL403, and their

formulations combined with CS-TPP nanoparticles. The NPX concentrations tested were 0.5, 1, 2, and 4 mM. PL407 or PL407-PL403 control groups (with no NPX) were added to cell cultures at the same volume (0.2 mL) for the systems containing NPX. The molar ratio of drug to PL (NPX:PL) was 1:4 for all formulations tested. Cell viability was determined by a MTT reduction test, and the sample absorbance was determined at 570 nm. For morphological analysis, cells were seeded in 12-well plates (1.10^4 cells/well) and observed under an inverted microscope before and after staining with toluidine blue (0.05% m/v).

2.10.1. Statistical analysis

Data are expressed as the mean ± standard deviation and analyzed by one-way analysis of variance (One-way ANOVA) with a Tukey-Kramer test. The analyses were done using Graph Pad Prism (Graph Pad Software Inc., USA) and Origin 6.0 (Microcal™ Software, Inc., Northampton, MA, USA). Statistical differences were defined using $p < 0.05$.

3. Results and Discussion

3.1. Characterization of chitosan-tripolyphosphate nanoparticles (CS-TPP)

CS-TPP nanoparticles were characterized by their hydrodynamic diameter, mean distribution size, polydispersity index, and zeta potential, which are important parameters to consider for the development of colloidal carriers[26]. In general, the size distribution of the CS-TPP nanoparticles presented a main portion with a hydrodynamic diameter of 318.3 ± 30.6 nm (68.8 ± 3.2%) and a minor portion with a diameter of 92.4 ± 11.6 nm (31.2 ± 2.9%). After NPX incorporation, the nanoparticle dimensions were 230.2 ± 28.5 nm (76.3 ± 12.2%) and 108.66 ± 18.8 nm (21.2 ± 15.6%).

Reports have shown differences in the hydrodynamic diameters of CS-TPP nanoparticles as a function of the TPP concentration. This is related to the high availability of anionic groups in the preparation medium, which are capable of interacting with the positive amino-groups in CS[27]. Diameters of ~250 nm were observed at CS:TPP ratios of 0.16:0.15[27], 0.4:0.095[28], and 0.3:0.08[29]. Lower ratios of CS:TPP (0.1: 0.1) resulted in the formation of particles with ~300-nm diameter[24], which is consistent with the results reported in this work.

The polydispersion index was 0.261 ± 0.02, and the zeta potential was + 35 to 40 mV. These parameters are important information related to the nanoparticles' homogeneity and reduced aggregation due to the nanoparticle repulsion caused by the positive charges of CS. Positively charged particles tend to present enhanced bioadhesive properties[30]. These results agree with a previous study that reported a polydispersion index of 0.26 and positive zeta potential of + 21 mV[15] for CS-TPP nanoparticles cross linked with glutaraldehyde. In addition, the EE and DL percentages were 98.4 ± 0.3% and 36.9 ± 0.12%, respectively, which are important features for maintaining effective drug ratios in the intra-articular microenvironment.

3.2. Evaluation of NPX solubility limit in PL407 and PL407-PL403 solutions

Concentrations of 0.5–10% (m/v) PL407 or PL407-PL403 were used to determine the NPX solubility in the different formulations. For both systems, a linear increase in NPX solubility was observed ($R^2 = 0.95104$ and 0.95264 for PL407 and PL407-PL403, respectively), which indicates drug incorporation in the micelles. However, the highest NPX concentrations were observed after incorporation in the PL407-PL403 binary system (4.06–6.75 mM) and were statistically different from those observed for the PL407 system ($p < 0.01$). The differences in HLB values between PL407 (HLB = 22) and PL403 (HLB = 8)[31] and the incorporation of a more hydrophobic copolymer (PL403) are essential points for enhancing the drug solubility in the formulations.

The concentration of NPX added to the PL solutions was 10.86 mM (2.5 $mg.mL^{-1}$), which is based on the incorporated NPX percentages of 62.4% in PL407-PL403 and 51.6% in the PL407 systems. The solubilization process occurs by replacing the water in the micelle cores with the drug, and NPX presents low aqueous solubility (25 $mg.L^{-1}$)[32]. Thus, this factor favors the possible incorporation of the drug in the micellar core and increases the solubility in PL formulations. These results are consistent with other studies on the solubility and partitioning of NPX in micellar phases with different surfactants, such as Brij, CTAB, SDS[27], and PL407[33, 34].

3.3. Micellar hydrodynamic diameters and size distribution: drug-micelle interaction and its influence on PL 407 and PL407/PL403 systems

The micellar hydrodynamic diameter, mean size distribution, and polydispersity were evaluated for all PL-systems in the presence and absence of CS-TPP nanoparticles and NPX at 25 and 37 °C. At 25 °C, the hydrodynamic diameter of the PL407 micelles was mostly ~45 nm (88%) and a minor portion with ~5-nm diameter (12%). The micellar dimensions of PL407-PL403 before and after NPX incorporation were 42 nm and 46 nm (both 95%), respectively. However, increasing the temperature resulted in changes in those parameters. At 37 °C, the micellar diameters were 23–30 nm for both PL407 and PL407-403 (~100% mean distribution). The polydispersion index values were 0.5–0.2 at 25 and 37 °C, respectively, indicating homogeneity and organization of the micellar systems.

Reductions in the micellar hydrodynamic diameter are directly related to the increase of temperature, which promoted by the dehydration of propylene oxide (PPO) units in the micellar core[35]. Moreover, the increase in temperature also influences the hydrophobicity of the micellar core by favoring the formation of a colloidal system with low polydispersivity[36]. *There are similar results reporting the influence of temperature on PL micelles composed of a single polymer (PL 407)*[34, 37] *and also for other types of PL407-based particles such as, PL407-polyethylenimine*[38].

These observations can be applied to micelles composed of isolated PL407 or combined with PL403. Despite the

difference in hydrophobicity (Hidrophilic Lipophilic Balance-HLB of 22 for PL407 and HLB = of 8 for PL 403), the number of PPO units is similar (65 and 69 for PL 407 and PL 40, respectively). This demonstrates that there are no significant differences in hydrodynamic diameter. The incorporation of NPX in the PL407-PL403 binary systems also changed the micellar hydrodynamic diameter, which demonstrates the probable influence of NPX incorporation in the micellar core. In general, the highest hydrodynamic diameter values were found for the formulations containing the dispersed CS-TPP nanoparticles in micellar systems (220.4 ± 0.850 at 25 °C and 233.63 ± 6.26 at 37 °C), with polydispersity indexes between 0.2 and 0.4. The temperature variation did not change the diameter of the CS-TPP nanoparticles and were only different for the micellar systems, even in the presence of NPX.

3.4. Differential Scanning Calorimetry (DSC) and rheological analysis

The temperatures and enthalpy variation in relation to the micellization process were determined by DSC. Table 1 shows the values for Tonset, Tm, Tendset, and enthalpy (ΔHm) for the different formulations. Thermal analysis of the CS-TPP nanoparticles showed no peaks related to the phase transitions, even after NPX incorporation. However, the analysis of the hydrogels presented endothermic peaks with a small displacement related to the increase in the copolymer concentration and the variations in the composition of the hydrogels (PL407 or PL407-PL403). Representative thermograms are available on Supporting Information.

The DSC analysis also showed that Tm, ΔH°, and ΔG° were similar for all formulations. For all formulations, thermograms presented two peaks corresponding to the micelles formation and aggregation in solution[39]. The Tm values for PL-based systems were ∼12–26 °C, depending on the PL type and NPX incorporation. In addition, for PL 403 systems, Tm was reduced by about 2–5 °C, and the ΔHm values decreased by approximately 0.5 J/g when compared to the system containing only PL407 (20%). This suggests an essential influence of PL403 on micelles self-assembly.

Table 1. Temperatures (T) and enthalpy variation (ΔH) relative to the micellization for PL-based hydrogels.

Formulations	Tonset (°C)	Tm (°C)	Tendset (°C)	ΔH (J/g)
CS-TPP	–	–	–	–
CS-TPP-NPX	–	–	–	–
18%				
PL407	14.0	17.3	25.9	2.2
PL407-NPX	13.7	18.2	28.3	2.7
PL407-CS-TPP	–	–	–	–
PL407-CS-TPP-NPX	12.0	17.1	24.8	3.2
20%				
PL407	12.9	16.7	26.1	3.1
PL407-NPX	12.5	16.6	26.8	3.0
PL407-CS-TPP	9.4	14.4	21.1	2.2
PL407-CS-TPP-NPX	11.4	15.8	23.2	3.6
18-2%				
PL407-PL403	12.0	16.0	23.7	2.8
PL407-PL403-NPX	10.5	15.6	21.8	2.6
PL407-PL403-CS-TPP	8.9	13.8	21.0	2.5
PL407-PL403-CS-TPP-NPX	9.7	14.7	23.7	3.5

Tonset, Tm and Tendset are the initial, peak and final micellization temperatures, respectively.

The results highlight that the incorporation of CS-TPP nanoparticles in the hydrogels promoted significant interference on polymeric systems self-organization, showing reduced Tm and ΔH values. However, the most significant effect of CS-TPP addition to the hydrogels was observed for PL407 (18%), which made the hydrogels thermosensitive. When the NPX was incorporated in the PL407-CS-TPP (20%) or PL407-PL403-CS-TPP (18-2%) hydrogels, the relative micellization temperature and the enthalpy variation increased, as a probable result from shifting the hydrogel self-assembly by the insertion of NPX-CS-TPP, which changed the systems structural organization due to possible interaction of the PL with the CS-TPP networks, as also described by a previous study[39].

Rheological analysis was performed for all formulations while considering their different compositions, the CS-TPP nanoparticle incorporation, and the presence or absence of NPX. The analysis made it possible to determine the elastic (G′) and viscous (G″) modulus, the viscosity (η), and the sol-gel transition temperature (Tsol-gel). Figure 1 shows representative rheograms for PL407-PL403 hydrogels and their analysis with respect to temperature and frequency.

The rheological profiles for CS-TPP nanoparticles presented no changes in G′, G″, and viscosity, which shows that the nanoparticles are not thermosensitive systems (Figures 1A and 1B). However, the hydrogels composed of PL407 alone or in a binary system with PL403 presented viscoelastic behavior, with G′ predominating over G″ (Figures 1C and 1D). In general, G″ showed an unstable profile, but the oscillations seem to be reduced after adding PL403 (2%) to the formulation.

The effects of CS-TPP nanoparticle incorporation in the hydrogels were more pronounced for PL407 systems at 18%, which changed the behavior from non-Newtonian above the gelation temperature to Newtonian behavior. The incorporation also affected the viscosity values (Table 2). Furthermore, CS-TPP incorporation in the PL407 hydrogels reduced G′ when compared to the isolated PL407 system (Table 2). This probably occurred by disturbing the micelle-micelle interactions and the hydrogels structural organization. In contrast, for PL403-PL407 hydrogels, there were no pronounced shifts after the addition of CS-TPP nanoparticles (Figures 1E and 1F).

The differences between G′ and G″ after PL403 addition can be attributed to their physico-chemical properties, such as a lower HLB value (HLB = 8) in relation to PL407 (HLB = 22). These properties provide stabilization in the structural organization of the hydrogels. The addition of NPX improved G′ and led to high G′/G″ relationships for the 20% PL407 and 18-2% PL407-PL403 systems (Table 2). This was probably due to the drug insertion in the hydrogels systems. The viscosity showed constant values at up to 20 °C but the increased after this point until the sol-gel transition phase, which occurred between 28 and 32 °C. These results support reports in the literature, where high PL407 concentrations showed Tsol-gel between ∼25 and 33 °C[40]. In fact,

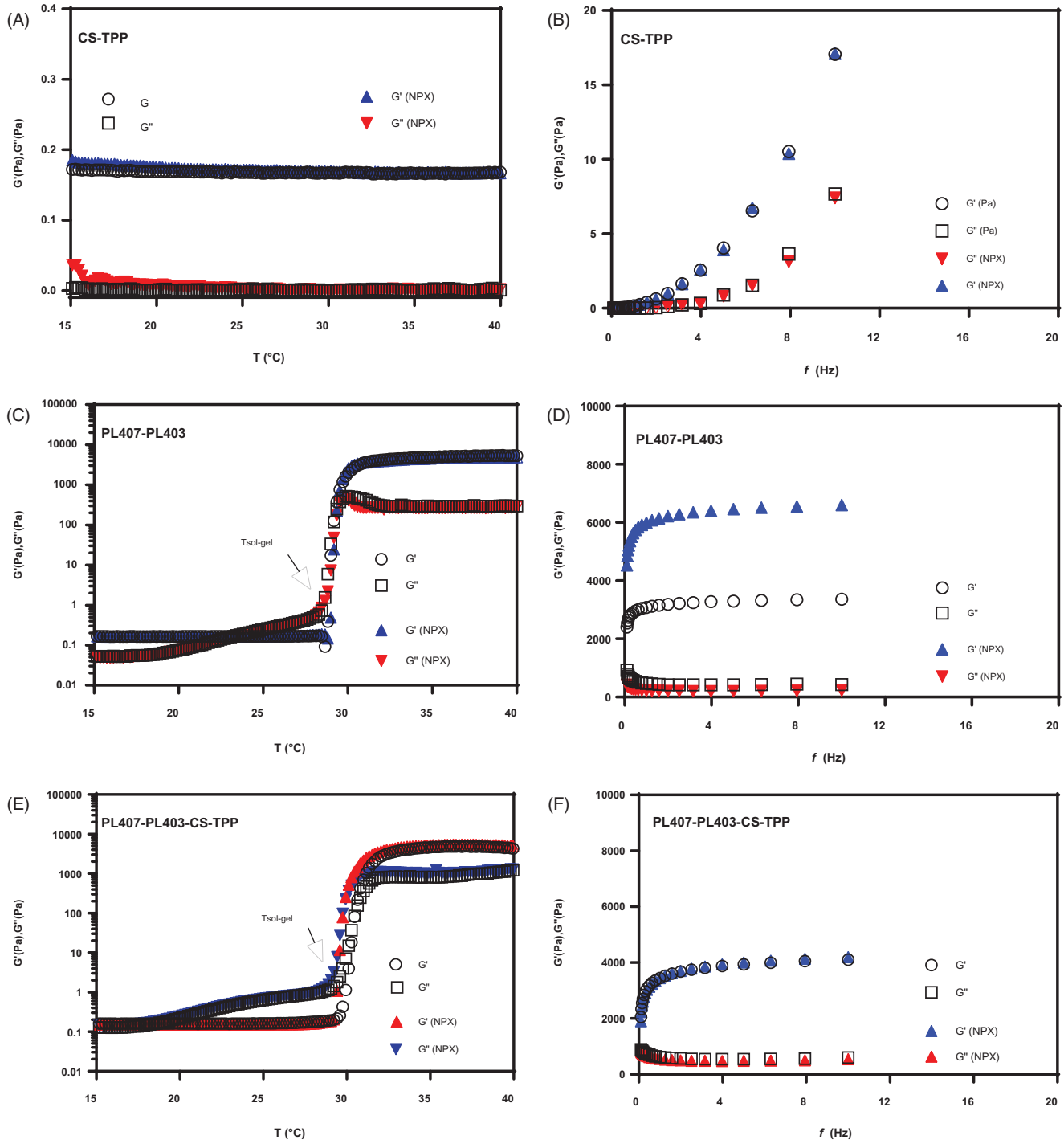

Figure 1. Representative rheograms obtained for CS-TPP nanoparticles (A, B), PL407-PL403 (C, D) and PL407-PL403-CS-TPP (E, F) hydrogels before and after NPX incorporation, against temperature and frequency sweep analyzes.

previous reports in the literature presented discussions about the influence of other polymers and solutes on PL sol-gel transition phenomenon. The unique properties of PL binary systems can be attributed to their capability for forming mixed micelles (for PL with similar PEO chains lengths but different PPO blocks lengths) and/or the coexistence of micelles populations composed of each PL independently[41], being essential for gelling process. In the case of PL407 and PL403, differences on their PEO:PPO relationships (~3:1 and 1:5, respectively) can also influence on sol-gel transition temperature variations, since micelles aggregations seems to be dependent on PPO chains assembly[41]. Additionally, hydrogels formed by PL with different HLB values creates systems with particular physico-chemical properties, structurally influenced by the presence of ions, co-solutes[42] and also nanoparticles[39].

3.5. Supramolecular structure and release kinetics

Figure 2 presents the SAXS results obtained for all hydrogels before and after the incorporation of CS-TPP nanoparticles and NPX. The results show the presence of a hexagonal

Table 2. Elastic (G′) and viscous (G′) moduli, viscosity (η, mPa.s) at 25 °C and 37 °C and sol-gel transition temperatures (Tsol-gel, °C) for PL-CS-TPP nanoparticles hydrogels formulations

Formulations	G′ (Pa)	G″ (Pa)	G′/G″ (1 Hz)	(mPa.s, 25 °C)	(mPa.s, 37 °C)	Tsol-gel (°C)
CS-TPP	0.157	0.003	52.3	26.7	26.5	–
CS-TPP-NPX	0.165	0.004	41.2	25.3	25.1	–
18 %						
PL407	7740	575.9	13.4	7142	1,230,000	29.0
PL407-CS-TPP	0.165	0.04	4.1	2648	2628	–
PL407-NPX	9150	466.1	19.6	7224	1,458,000	24.9
PL407-CS-TPP-NPX	0.156	0.05	3.1	2481	2478	–
20 %						
PL407	9449	697.4	13.5	8121	1,508,000	27
PL407-CS-TPP	5079	473.9	10.7	9882	125,600	29
PL407-NPX	9037	626.2	14.4	8007	866,000	28
PL407-CS-TPP-NPX	5802	468.5	12.4	10,790	145,900	33
18-2%						
PL407-PL403	51930	1717	30.2	48,460	827,900	28
PL407-PL403-CS-TPP	48410	4227	11.4	48,660	771,600	31
PL407-PL403-NPX	48780	1393	35.0	109,300	790,600	29
PL407-PL403-CS-TPP-NPX	54090	1150	47.0	125,800	878,900	31

PL and CS-TPP refer to poloxamer and chitosan-tripolyphosphate nanoparticles.

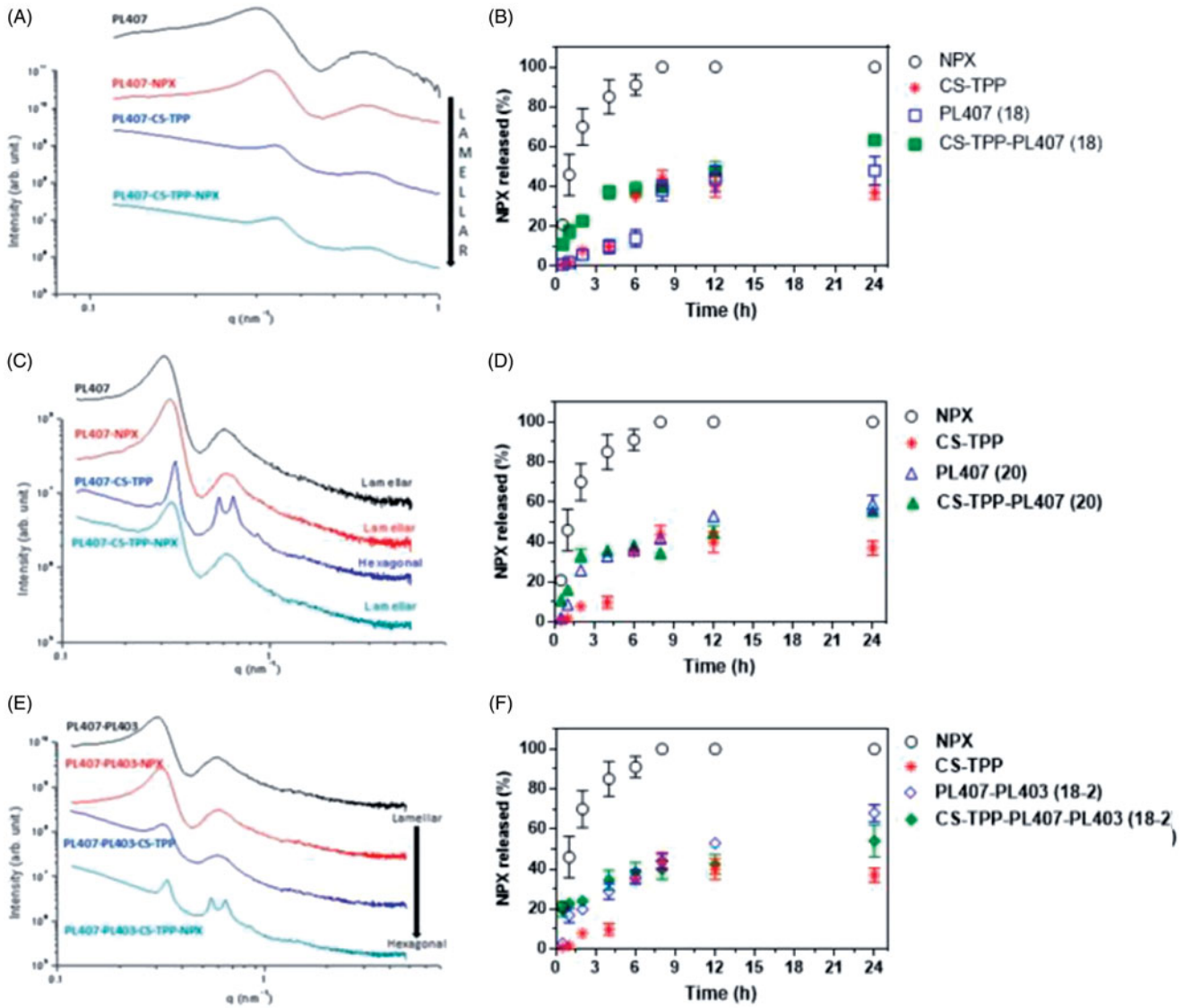

Figure 2. SAXS patterns obtained for 18% PL407 (A), 20% PL407 (C) and 18-2% PL407-PL403 (E) hydrogels before and after NPX or CS-TPP nanoparticles incorporation. NPX release profiles from are shown on panel A and D for 18 and 20% PL407, respectively, and panel F for 18-2% PL407-PL403 hydrogels before and after CS-TPP nanoparticles incorporation ($n = 6$/formulation).

structure with the following scattering peaks: q * (main peak), * √3q *, √4q *, and √7q *. The data were found through the relationship of q * value (main peak) to the relative position of the Bragg peaks from the scattering generated by the secondary planes. The symmetry of the three-dimensional arrangements could then be determined. For most systems, the results showed the presence of a lamellar structure (q * and √4q *), which was preserved after NPX incorporation in the PL407 (18 and 20%) and PL407-PL403 (18-2%) formulations.

The maintenance of the lamellar phase organization was observed for the PL407-CS-TPP systems at 18% PL407, even after NPX encapsulation in the nanoparticles. For 20% PL407, the incorporation of CS-TPP nanoparticles modified the system organization, which resulted in changes from hexagonal to lamellar phase. This this behavior was maintained for PL407-CS-TPP-NPX. For the PL407-PL403 system, the phase organization was shifted from lamellar to hexagonal following the addition of CS-TPP-NPX, indicating structural organization of the systems after drug encapsulation. Similar patterns were obtained for PL-based binary hydrogels containing different drugs, such as sumatriptan succinate[43], ropivacaine hydrochloride[44], and lidocaine[45].

Comparative analysis of the formulations containing 18 and 20% PL407 showed the influence of the final PL concentration on the system organization and their interactions with the CS-TPP nanoparticles. The hexagonal phase organization observed for 20% PL407-CS-TPP hydrogels showed a possible interaction of PL407 with the CS-TPP surfaces. However, the interaction was altered when encapsulating NPX in the CS-TPP nanoparticles, as indicated by the shifts from hexagonal to the lamellar phase organization.

In the presence of PL403, a more hydrophobic copolymer (HLB = 8) was observed in comparison to PL407 (HLB = 22), and there were no structural changes. However, SAXS analysis showed interesting results after the incorporation of CS-TPP nanoparticles. In the presence of encapsulated NPX, the phase organization of the system changed from lamellar to hexagonal. This can be explained by the possible adsorption of the drug in the CS-TPP surface allowing interactions with PL403 in the hydrogel formulation.

When drugs, salts, or polymers are incorporated in the PL systems, new supramolecular structures can be created due to their insertion in the intermicellar spaces[46]. Additionally, CS is a polymer with hydrophilic features, which lead to more pronounced hydration effects, especially for PL407-PL403 systems. This could explain the hydrogels structural changes in the presence of CS-TPP nanoparticles. In a previous study, the addition of lipophilic components such as triglycerides or vitamin A in systems based on glycerol oleate (GMO) and PL407 favored the formation of hexagonal structure[47]. In this case, PL407 was used as dispersant medium. However, the systems are quite sensitive and can undergo structural variations according to component changes, the addition of different drugs, solvent, pH, and stability over time[48]. In this context, the formation of body-centered cubic and hexagonal phases is reported for PL407 concentrations of 25 to 63 and 63 to 80% (w/v), respectively. However, the preparation method included a step for removing hydrophobic impurities using hexane solvent[49], which was not used for the formulations described in this work. This could explain the differences observed for the reported results. *In special, for other self-assembled systems, such as, cucurbit-8-uril, the solvent evaporation allowed the formation of hydrogels and microcrystals with frameworks driven by their aromatic units*[50].

The NPX release profiles from different formulations (CS-TPP nanoparticles and hydrogels) were evaluated using a two-compartment system separated by a cellulose acetate membrane (with MWCO 1000 Da.). The system contained artificial intra-articular fluid in the receptor medium to simulate physiological conditions for intra-articular administration. The results of the drug release assays are presented on Figure 2 and Table 3.

The NPX release from the solution was fast, and the final percentage (∼100% NPX released) occurred within 6–24 h. A regular release profile occurred during the whole period for the 18 and 20% PL407-NPX formulations or the combined PL407-PL403 (18-2%). The drug release percentages were lower than that of the NPX solution ($p < 0.001$). The results within 24 h were the following: 18% PL 407 (47.9 ± 7.1%); 20% PL 407 (58.9 ± 4.4%), 18-2% PL407-PL403 (67.9 ± 4.2%), CS-TPP nanoparticles (36.9 ± 3.5%), 18% PL407-CS-TPP nanoparticles (63.3 ± 1.8%), 20% PL407-CS-TPP nanoparticles (55.5 ± 1.5%), and 18-2% PL407-PL403-CS-TPP nanoparticles (54.2 ± 3.0%).

Table 3. Release constants and determination coefficients obtained for NPX release from PL407 and PL407-PL403 hydrogels before and after CS-TPP nanoparticles incorporation.

	Zero Order		Higuchi		Korsmeyer-Peppas		
Formulations	K_0 (%.h^{-1})	R^2	K_H (%.h$^{-1/2}$)	R^2	K_{KP} (%.h^{-n})	R^2	n
NPX*	11.4 ± 3.2	0.804	38.9 ± 7.2	0.907	1.58 ± 0.05	0.902	0.56
CS-TPP	5.6 ± 2.3	0.862	17.2 ± 5.3	0.779	0.36 ± 0.08	0.954	1.38
18 %							
PL407	3.9 ± 0.6	0.940	12.2 ± 2.7	0.872	0.93 ± 0.04	0.984	1.26
PL407-CS-TPP	5.5 ± 1.7	0.871	16.2 ± 1.3	0.719	0.33 ± 0.06	0.963	1.21
20 %							
PL407	5.9 ± 1.6	0.819	20.2 ± 3.6	0.914	0.83 ± 0.11	0.930	1.14
PL407-CS-TPP	4.3 ± 0.3	0.843	14.5 ± 1.8	0.726	0.30 ± 0.03	0.945	1.19
18-2 %							
PL407-PL403	5.1 ± 1.1	0.874	17.8 ± 2.6	0.833	0.75 ± 0.12	0.874	0.88
PL407-PL403-CS-TPP	4.0 ± 0.3	0.821	13.8 ± 0.9	0.787	0.26 ± 0.08	0.929	1.25

Data presented as mean ± S.D. (n = 3/formulation). *Sodium naproxen at 1 mg/mL (0.9% NaCl solution).

The release profiles were evaluated using mathematical models (Zero order, Higuchi, and Korsmeyer-Peppas). The results showed higher constant values (Krel) for NPX in solution than the formulations of PL407, PL407-PL403, CS-TPP nanoparticles, and CS-TPP nanoparticles combined with hydrogels. In general, the Krel values for hydrogel formulations were similar and followed the Korsmeyer-Peppas model, and the best correlation coefficients intervals were obtained ($R^2 = 0.87 \geq 0.98$), as shown in Table 3.

In order to understand the contribution to the release exponent (n), the Korsmeyer-Peppas model is used when the release mechanism is not well known or when there is a combination of two processes: drug transport that follows the Fick Law (diffusion) and when erosion is an important component to evaluate, as in the case of polymer matrices (which is considered as a relaxation of polymer chains). Thus, variations in the n value are described according to these mechanisms and the geometric form of the release matrix (carrier). When $n = 0.5$, the release mechanism corresponds to a Fickian diffusion, while $n = 0.89$ means that the drug release is controlled by the carrier erosion. When $n > 0.89$, there is a contribution of both processes, which is described as anomalous transport[51]. The drug diffusion and polymer chain relaxation are considered as essential factors for the NPX release from the hydrogels and CS-TPP nanoparticles. Thus, the possible mechanisms involved in the NPX release control *in vivo* refer to the dissolution and erosion of the hydrogel by synovial fluid at the site of administration, which are combined with the drug diffusion through the micelles until possibly reaching the bloodstream.

3.6. Cell viability assays

Cell viability assays were done with fibroblasts (VERO) and osteoblasts (MC3T3) using isolated PL407 formulations or combined with PL403 in the presence or absence of CS-TPP nanoparticles and NPX. Positive (phenol 0.25%) and negative controls (cultured cells in culture plates and treated with DMEM medium only) were also examined, as presented on Figure 3 (graphs and micrographs). In general, all formulations were significantly different from the positive control ($p < 0.001$), which resulted in different cytotoxic effects for both cell lines.

The cell viability values did not decrease after treatment with PL407 formulations. NPX incorporation and CS-TPP nanoparticles did not alter the cell viability profiles and presented similar results to the negative control (non-cytotoxic). Those results suggest the biocompatibility of the systems CS-TPP-PL-hydrogels, as also observed for other types of polymeric carries, including polylactic acid-metal complexes (gold, silver, zinc, magnesium)[52], polylactic acid-chitosan nanofibers[53] and polyethylene glycol-serum bovine albumin[54], in different cells line such as human bone marrow (UE7T-13) and HeLa. Additionally, results obtained from the Vero and MC3T3 cell lines showed that treatment with

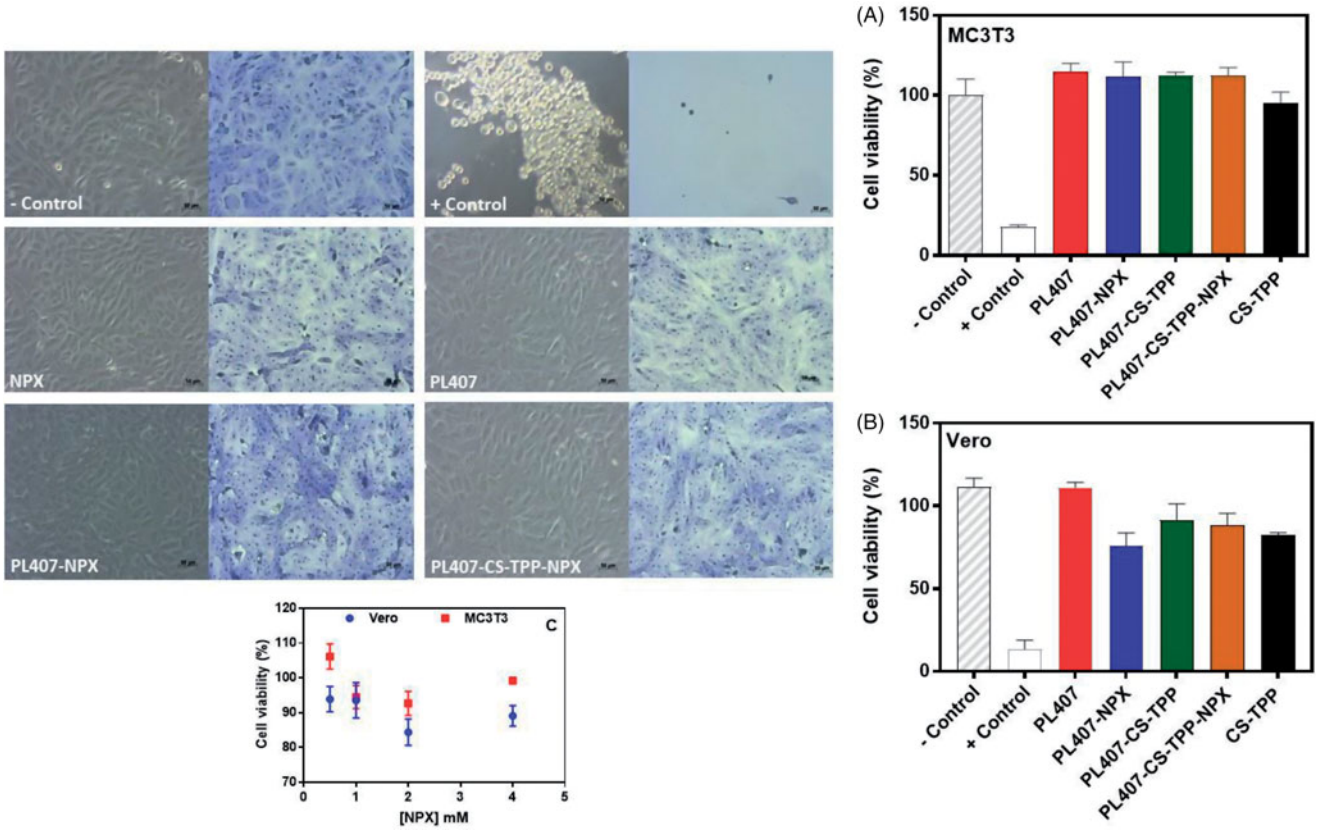

Figure 3. Effects PL407 hydrogels (A- MC3T3 cells and B- Vero cells) and NPX (C) evaluated by MTT reduction test. Positive control (+ control = 0.25% phenol) and negative control (- control = cells seeded in culture medium). Micrographs obtained after direct cytotoxicity assay. Phase contrast microscopy and toluidine blue staining. Note the presence of reduced cells number for positive control.

NPX did not reduce cell viability (Figures 3A, B and C). However, the combined PL407-PL403-CS-TPP-NPX reduced the cell viability percentage in comparison to the PL407 formulations ($p < 0.001$ for MC3T3 cells).

The reduction in cell viability after treatment with PL407-403 formulations could be related to the possible cellular uptake of hydrophobic PL, as observed by Gu et al.[55] for cells with the MDR phenotype. Furthermore, it may also be associated with constant drug release after the incorporation in CS-TPP in PL407-PL403 hydrogels. No cytotoxic effects were reported for PL403 after treating glioblastoma cells[56], which highlights possibilities for future *in vivo* investigations.

4. Final Considerations and Perspectives

The intra-articular administration of new pharmaceutical formulations could reduce the drug uptake to the systemic circulation and maintain it in the synovial fluid at clinically relevant concentrations. In order to achieve this goal, we presented the development of PL-based hybrid hydrogels containing NPX in CS-TPP nanoparticles and considered their structural characterization, drug release performance, and effects on two different cell lines. The addition of CS-TPP nanoparticles to the hydrogels shifted the micellization temperatures and enthalpy variation, possibly by interfering in the micellar self-assembly and hydrogel formation due to possible interactions between PL and CS networks surrounding the nanoparticles.

In order to confirm this hypothesis, SAXS assays provided information about the hexagonal phase organization obtained for 20% PL407-CS-TPP nanoparticles. However, the PL-based systems supramolecular structures changed after NPX or CS-TPP nanoparticle incorporation, which showed hexagonal phases depending on the hydrogels compositions. In the presence of PL403, a more hydrophobic copolymer (HLB = 8) than PL407 (HLB = 22), the phase organization shifted from lamellar to hexagonal, where NPX low release constants were observed for both phase organizations. Those results indicate that there is a possible drug adsorption on the CS-TPP nanoparticle surfaces, which allowed interaction with PL403 in the surrounding hydrogel system. The rheological characterization of the hydrogels showed that the formulations presented a well-organized structure indicated by high G′/G″ values. *In vitro* release assays revealed that the associated CS-TPP-PL hydrogels induced low NPX release constants, as a contribution of the drug diffusion and polymeric chain relaxation for release mechanisms, suggesting that slow drug uptake from the synovial cavity would occur. Finally, the cell viability assays showed low cytotoxic effects, especially for PL407 systems, which makes the systems promising matrices for possible NPX intra-articular release.

Funding

This research work was supported by Coordenação de Aperfeiçoamento de Pessoal de Nível Superior (CAPES), Fundação de Amparo à Pesquisa do Estado de São Paulo [FAPESP 2014/26200-9, 2014/14457-5, 2014/12653-1] and Conselho Nacional de Desenvolvimento Científico e Tecnológico [CNPq 309207/2016-9, 402838/2016-5]. Authors are also grateful to the Brazilian Synchrotron Light Laboratory for SAXS facilities (SAXS 1 beamline) and UFABC Multiuser Central Facilities (CEM-UFABC).

References

[1] Seed, M. P.; Gardner, C. R. The Modulation of Intra-Articular Inflammation, Cartilage Matrix and Bone Loss in Mono-Articular Arthritis Induced by Heat-Killed Myobacterium Tuberculosis. *Inflammopharmacol.* **2005**, *12*, 551–567. DOI: 10.1163/156856005774382607.

[2] Grespan, R.; Fukada, S. Y.; Lemos, H. P.; Vieira, S. M.; Napimoga, M. H.; Teixeira, M. M.; Fraser, A. R.; Liew, F. Y.; McInnes, I. B.; Cunha, F. Q. CXCR2-Specific Chemokines Mediate Leukotriene B(4)-Dependent Recruitment of Neutrophils to Inflamed Joints in Mice with Antigen-Induced Arthritis. *Arthritis Rheum.* **2008**, *58*, 2030–2040. DOI: 10.1002/art.23597.

[3] Botting, R. M. Inhibitors of Cyclooxygenases: mechanisms, Selectivity and Use. *J. Physiol. Pharmacol.* **2006**, *57*, 113–124.

[4] Jaffré, B.; Watrin, A.; Loeuille, D.; Gillet, P.; Netter, P.; Laugier, P.; Saïed, A. Effects of Antiinflamatory Drugs on Arthritic Cartilage: A High-Frequency Quantitative Ultrasound Study in Rats. *Arthritis Rheum.* **2003**, *48*, 1594–1601. DOI: 10.1002/art.11023.

[5] Lin, J.; Zhang, W.; Jones, A.; Doherty, M. Efficacy of Topical Non-Steroidal anti-Inflammatory Drugs in the Treatment of Osteoarthritis: Meta-Analysis of Randomised Controlled Trials. *BMJ* **2004**, *329*, 324–330. DOI: 10.1136/bmj.38159.639028.7C.

[6] Okur, N. Ü.; Ege, M. A.; Karasuluh, Y. Preparation and Characterization of Naproxen Loaded Microemulsion Formulations for Dermal Application. *Int. J. Pharm.* **2014**, *4*, 33–42.

[7] Tian, Q.; Ren, F.; Xu, Z.; Xie, Y.; Zhang, S. Preparation of high solubilizable microemulsion of naproxen and its solubilization mechanism. *Int. J. Pharm.* **2012**, *426*, 202–210. DOI: 10.1016/j.ijpharm.2012.01.019.

[8] Essving, P.; Axelsson, K.; Kjellberg, J.; Wallgren, O.; Gupta, A.; Lundin, A. Reduced Hospital Stay, Morphine Consumption and Pain Intensity with Local Infiltration Analgesia after Unicompartmental Knee Arthroplasty. *Acta Orthop.* **2009**, *80*, 213–219. DOI: 10.3109/17453670902930008.

[9] Thing, M.; Larsen, C.; Østergaard, J.; Jensen, H.; Larsen, S. W. In Vitro Release from Oil Injectables for Intra-Articular Administration: Importance of Interfacial Area, Diffusivity and Partitioning. *Eur. J. Pharm. Sci.* **2012**, *45*, 351–357. DOI: 10.1016/j.ejps.2011.12.006.

[10] Thing, M.; Lu, Y.; Ågårdh, L.; Larsen, C.; Østergaard, J.; He, W.; Wu, W.; Larsen, F. F.; Larsen, S. W. Prolonged Naproxen Joint Residence Time after Intra-Articular Injection of Lipophilic Solutions Comprising a Naproxen Glycolamide Ester Prodrug in the Rat. *Int. J. Pharm* **2013**, *451*, 34–40. DOI: 10.1016/j.ijpharm.2013.04.056.

[11] Bozdağ, S.; Caliş, S.; Kaş, H. S.; Ercan, M. T.; Peksoy, I.; Hincal, A. A. In Vitro Evaluation and Intra-Articular Administration of Biodegradable Microspheres Containing Naproxen Sodium. *J. Microencapsul.* **2001**, *18*, 443–456.

[12] Larsen, S. W.; Østergaard, J.; Friberg-Johansen, H.; Jessen, M. N.; Larsen, C. In Vitro Assessment of Drug Release Rates from Oil Depot Formulations Intended for Intra-Articular Administration. *Eur. J. Pharm. Sci.* **2006**, *29*, 348–354. DOI: 10.1016/j.ejps.2006.07.002.

[13] Morgen, M.; Tung, D.; Boras, B.; Miller, W.; Malfait, A. M.; Tortorella, M. Nanoparticles for Improved Local Retention after Intra-Articular Injection into Knee Joint. *Pharm. Res.* **2013**, *30*, 257–268. DOI: 10.1007/s11095-012-0870-x.

[14] Ryan, S. M.; Mcmorrow, J.; Umerska, A.; Patel, H. B.; Kornerup, K. N.; Tajber, L.; Murphy, E. P.; Perretti, M.; Corrigan, O. I.; Brayden, D. J. An Intra-Articular Salmon Calcitonin-Based Nanocomplex Reduces Experimental Inflammatory Arthritis. *J. Control. Release* **2013**, *167*, 120–129. DOI: 10.1016/j.jconrel.2013.01.027.

[15] Russo, E.; Gaglianone, N.; Baldassari, S.; Parodi, B.; Croce, I.; Bassi, A. M.; Vernazza, S.; Caviglioli, G. Chitosan-Clodronate Nanoparticles Loaded in Poloxamer Gel for Intra-Articular Administration. *Coll. Surf. B Biointerfaces* **2016**, *143*, 88–96. DOI: 10.1016/j.colsurfb.2016.03.028.

[16] Kang, M. L.; Ko, J. Y.; Kim, J. E. Im, G.I. Intra-Articular Delivery of Kartogenin-Conjugated Chitosan Nano/Microparticles for Cartilage Regeneration. *Biomaterials* **2014**, *1*, 9984–9994.

[17] Zhou, G.; Niepel, M. S.; Saretia, S.; Groth, T. Reducing the Inflammatory Responses of Biomaterials by Surface Modification with Glycosaminoglycan Multilayers. *J. Biomed. Mater. Res. A* **2016**, *104*, 493–502. DOI: 10.1002/jbm.a.35587.

[18] Yang, Y.; Guo, Q. F.; Peng, J. R.; Su, J.; Lu, X. L.; Zhao, Y. X.; Qian, Z. Y. Doxorubicin-Conjugated Heparin-Coated Superparamagnetic Iron Oxide Nanoparticles for Combined Anticancer Drug Delivery and Magnetic Resonance Imaging. *J. Biomed. Nanotechnol.* **2016**, *12*, 1963–1974. DOI: 10.1166/jbn.2016.2298.

[19] Qu, Y.; Chu, B. Y.; Shi, K.; Peng, J. R.; Qian, Z. Y. Recent Progress in Functional Micellar Carriers with Intrinsic Therapeutic Activities for Anticancer Drug Delivery. *J. Biomed. Nanotechnol.* **2017**, *13*, 1598–1618. DOI: 10.1166/jbn.2017.2475.

[20] Lu, Z.; Huang, F.-Y.; Cao, R.; Lin, Y.-Y.; Zhou, S.; Zhao, H.; Huang, Y.; Zhang, L.; Tan, G.-H. Synthesis of mPEG-dBSA-Cy5.5 Nanoparticles for Tumor Imaging and Drug Delivery. *Nanosci. Nanotechnol. Lett.* **2017**, *9*, 184–189. DOI: 10.1166/nnl.2017.2277.

[21] Ahmad, R.; Deng, Y.; Singh, R.; Hussain, M.; Shah, M. A. A.; Elingarami, S.; He, N.; Sun, Y. Cutting Edge Protein and Carbohydrate-Based Materials for Anticancer Drug Delivery. *J. Biomed. Nanotechnol.* **2018**, *14*, 20–43. DOI: 10.1166/jbn.2018.2476.

[22] Li, F.; Jin, L.; He, L.; Deng, Y.; He, N. Nanoparticles Applied for Therapy and Diagnosis in Common Diseases. *Sci. Adv. Mater.* **2015**, *7*, 2103–2122. DOI: 10.1166/sam.2015.1982.

[23] Jin, L.; Zeng, X.; Liu, M.; Deng, Y.; He, N. Current Progress in Gene Delivery Technology Based on Chemical Methods and Nano-Carriers. *Theranostics* **2014**, *4*, 240–255. DOI: 10.7150/thno.6914.

[24] Grillo, R.; Pereira, A. E.; Nishisaka, C. S.; de Lima, R.; Oehlke, K.; Greiner, R.; Fraceto, L. F. Chitosan/Tripolyphosphate Nanoparticles Loaded with Paraquat Herbicide: An Environmentally Safer Alternative for Weed Control. *J. Hazard. Mater.* **2014**, *278*, 163–171. DOI: 10.1016/j.jhazmat.2014.05.079.

[25] Asasutjarit, R.; Thanasanchokpibull, S.; Fuongfuchat, A.; Veeranondha, S. Optimization and Evaluation of Thermoresponsive Diclofenac Sodium Ophthalmic in Situ Gels. *Int. J. Pharm* **2011**, *411*, 128–135. DOI: 10.1016/j.ijpharm.2011.03.054.

[26] Konecsni, K.; Low, N. H.; Nickerson, M. T. Chitosan-Tripolyphosphate Submicron Particles as the Carrier of Entrapped Rutin. *Food Chem.* **2012**, *134*, 1775–1779. DOI: 10.1016/j.foodchem.2012.03.070.

[27] Cerchiara, T.; Abruzzo, A.; di Cagno, M.; Bigucci, F.; Bauer-Brandl, A.; Parolin, C.; Vitali, B.; Gallucci, M. C.; Luppi, B. Chitosan Based Micro- and Nanoparticles for Colon-Targeted Delivery of Vancomycin Prepared by Alternative Processing Methods. *Eur. J. Pharm. Biopharm.* **2015**, *92*, 112–119. DOI: 10.1016/j.ejpb.2015.03.004.

[28] Bahreini, E.; Aghaiypour, K.; Abbasalipourkabir, R.; Mokarram, A. R.; Goodarzi, M. T.; Saidijam, M. Preparation and Nanoencapsulation of L-Asparaginase II in Chitosan-Tripolyphosphate Nanoparticles and in Vitro Release Study. *Nanoscale Res. Lett.* **2014**, *9*, 340. DOI: 10.1186/1556-276X-9-340.

[29] Al-Kassas, R.; Wen, J.; Cheng, A. E.; Kim, A. M.; Liu, S. S. M.; Yu, J. Transdermal Delivery of Propranolol Hydrochloride through Chitosan Nanoparticles Dispersed in Mucoadhesive Gel. *Carb. Polym.* **2016**, *153*, 176–186. DOI: 10.1016/j.carbpol.2016.06.096.

[30] Kumar, S. P.; Birundha, K.; Kaveri, K.; Devi, K. T. R. Antioxidant Studies of Chitosan Nanoparticles Containing Naringenin and Their Cytotoxicity Effects in Lung Cancer Cells. *Int. J. Biol. Macromol.* **2015**, *78*, 87–95. DOI: 10.1016/j.ijbiomac.2015.03.045.

[31] Chiappetta, D. A.; Sosnik, A. Poly(Ethylene Oxide)-Poly(Propylene Oxide) Block Copolymer Micelles as Drug Delivery Agents: improved Hydrosolubility, Stability and Bioavailability of Drugs. . *Eur. J. Pharm. Biopharm.* **2007**, *66*, 303–317. DOI: 10.1016/j.ejpb.2007.03.022.

[32] Cirri, M.; Maestrelli, F.; Corti, G.; Furlanetto, S.; Mura, P. Simultaneous Effect of Cyclodextrin Complexation, pH, and Hydrophilic Polymers on Naproxen Solubilization. *J. Pharm. Biomed. Anal.* **2006**, *42*, 126. DOI: 10.1016/j.jpba.2005.11.029.

[33] Bhat, P. A.; Dar, A. A.; Rather, G.; M. Effect of Surfactant Mixing on Partitioning of Model Hydrophobic Drug, Naproxen, Between Aqueous and Micellar Phases. *J. Phys. Chem. B* **2009**, *113*, 997–1006. DOI: 10.1021/jp807229c.

[34] Sharma, P. K.; Bhatia, S. K. Effect of anti-inflammatories on Pluronic F127: micellar assembly, gelation and partitioning . *Int. J. Pharm.* **2004**, *278*, 361–377. DOI: 10.1016/j.ijpharm.2004.03.029.

[35] Zhang, Y.; Lam, Y. M.; Tan, W. S. Poly(Ethylene Oxide)-Poly(Propylene Oxide)-Poly(Ethylene Oxide)-g-Poly(Vinylpyrrolidone): Association Behavior in Aqueous Solution and Interaction with Anionic Surfactants. *J. Coll. Int. Sci.* **2005**, *285*, 74–79. DOI: 10.1016/j.jcis.2004.12.033.

[36] Su, Y. L.; Wang, J.; Liu, H. Z. FTIR Spectroscopic Study on Effects of Temperature and Polymer Composition on the Structural Properties of PEO-PPO-PEO Block Copolymer Micelles. *Langmuir* **2002**, *18*, 5370–5374. DOI: 10.1021/la020007p.

[37] Ricardo, N. M.; Pinho, M. E.; Yang, Z.; Attwood, D.; Booth, C. Controlling the Gelation of Aqueous Micellar Solutions of Ethylene-Oxide-Based Block Copoly(Oxyalkylene)s. *Int. J. Pharm.* **2005**, *300*, 22–31. DOI: 10.1016/j.ijpharm.2005.04.023.

[38] Teng, Y.; Shen, X.; Zheng, L.; Gong, T.; Sun, Y.; Duan, Y. Synthesis of Gold-Nanoshelled Pluronic-PEI Nanocapsules for Drug Delivery. *J. Nanosci. Nanotechnol.* **2016**, *16*, 12154–12160. DOI: 10.1166/jnn.2016.12965.

[39] Ravani, L.; Esposito, E.; Bories, C.; Moal, V. L.; Loiseau, P. M.; Djabourov, M.; Cortesi, R.; Bouchemal, K. Clotrimazole-Loaded Nanostructured Lipid Carrier Hydrogels: thermal Analysis and in Vitro Studies. *Int. J. Pharm.* **2013**, *45*, 695–702. DOI: 10.1016/j.ijpharm.2013.06.015.

[40] Dorraj, G.; Moghimi, H. R. Preparation of SLN-Containing Thermoresponsive: In Situ Forming Gel as a Controlled Nanoparticle Delivery System and Investigating Its Rheological, Thermal and Erosion Behavior. *Iran J. Pharm. Res.* **2015**, *14*, 347–358.

[41] Zhang, M.; Djabourov, M.; Bourgaux, C.; Bouchemal, K. Nanostructured Fluids from Pluronic® Mixtures. *Int. J. Pharm.* **2013**, *454*, 599–610. DOI: 10.1016/j.ijpharm.2013.01.043.

[42] Roques, C.; Bouchemal, K.; Ponchel, G.; Fromes, Y.; Fattal, E. Parameters Affecting Organization and Transfection Efficiency of Amphiphilic Copolymers/DNA Carriers. *J. Control. Rel.* **2009**, *138*, 71–77. DOI: 10.1016/j.jconrel.2009.04.030.

[43] Oshiro, A.; Da Silva, D. C.; De Mello, J. C.; De Moraes, V. W.; Cavalcanti, L. P.; Franco, M. K. K. D.; Alkschbirs, M. I.; Fraceto, L. F.; Yokaichiya, F.; Rodrigues, T.; De Araujo, D. R. Pluronics F-127/L-81 Binary Hydrogels as Drug-Delivery Systems: influence of Physicochemical Aspects on Release

Kinetics and Cytotoxicity. *Langmuir* **2014**, *30*, 13689–13698. DOI: 10.1021/la503021c.

[44] Akkari, A. C. S.; Campos, E. V. R.; Kepler, A. F.; Fraceto, L. F.; de Paula, E.; de Araujo, D. R. Budesonide-Hydroxypropyl-β-Cyclodextrin Inclusion Complex in Binary Poloxamer 407/403 System for Ulcerative Colitis Treatment: A Physico-Chemical Study from Micelles to Hydrogels. *Coll. Surf. B Biointerfaces* **2016**, *138*, 138–147. DOI: 10.1016/j.colsurfb.2015.11.048.

[45] Nascimento, M. H. M.; Franco, M. K. K. D.; Yokaichyia, F.; de Paula, E.; Lombello, C. B.; de Araujo, D. R. Hyaluronic Acid in Pluronic F-127/F-108 Hydrogels for Postoperative Painin Arthroplasties: influence on Physicochemical Properties and Structural Requirements for Sustained Drug-Release. *Int. J. Biol. Macromol.* **2018**, *111*, 1245–1254. DOI: 10.1016/j.ijbiomac.2018.01.064.

[46] Salim, M.; Wan Iskandar, W. F. N.; Patrick, M.; Zahid, N. I.; Hashim, R. Swelling of Bicontinuous Cubic Phases in Guerbet Glycolipid: effects of Additives. *Langmuir* **2016**, *32*, 5552−−5561. DOI: 10.1021/acs.langmuir.6b01007.

[47] Gustafsson, J.; Nylander, T.; Almgren, M.; Ljusberg-Wahren, H. Phase Behavior and Aggregate Structure in Aqueous Mixtures of Sodium Cholate and Glycerol Monooleate. *J. Coll. Interf. Sci.* **1999**, *211*, 326–335. DOI: 10.1006/jcis.1998.5996.

[48] Kuntsche, J.; Jennifer, C.; Horst, J. C.; Bunjes, H. Cryogenic Transmission Electron Microscopy (cryo-TEM) for Studying the Morphology of Colloidal Drug Delivery Systems. *Int. J. Pharm.* **2011**, *417*, 120–137. DOI: 10.1016/j.ijpharm.2011.02.001.

[49] Liu, T.; Chu, B. Formation of Homogeneous Gel-like Phases by Mixed Triblock Copolymer Micelles in Aqueous Solution: FCC to BCC Phase Transition. *J. Appl. Crystallogr.* **2000**, *33*, 727–730. DOI: 10.1107/S0021889899013369.

[50] Tian, J.; Yao, C.; Yang, W.-L.; Zhang, L.; Zhang, D.-W.; Wang, H.; Zhang, F.; Liu, Y.; Li, Z.-T. In Situ-Prepared Homogeneous Supramolecular Organic Framework Drug Delivery Systems (sof-DDSs): Overcoming Cancer Multidrug Resistance and Controlled Release. *Chinese Chem. Lett.* **2017**, *28*, 798–806. DOI: 10.1016/j.cclet.2017.01.010.

[51] Costa, P.; Lobo, J. M. S. Modeling and Comparison of Dissolution Profiles. *Eur. J. Pharm. Sci.* **2001**, *13*, 123–133. DOI: 10.1016/S0928-0987(01)00095-1.

[52] Le, N. H.; Ritchie, J.; Sun, J. Shape Optimisation of Biocompatible/Degradable Helical Micro/Nano-Structures for Drug Delivery. *Nanosci. Nanotechnol. Lett.* **2017**, *9*, 495–500.

[53] Ji, X.; Yang, W.; Wang, T.; Mao, C.; Guo, L.; Xiao, J.; He, N. Coaxially Electrospun Core/Shell Structured Poly(L-Lactide) Acid/Chitosan Nanofibers for Potential Drug Carrier in Tissue Engineering. *J. Biomed. Nanotechnol.* **2013**, *9*, 1672–1678. DOI: 10.1166/jbn.2013.1665.

[54] Zhang, L.; Lu, Z.; Li, X.; Deng, Y.; Zhang, F.; Ma, C.; He, N. Methoxy Poly(Ethylene Glycol) Conjugated Denatured Bovine Serum Albumin Micelles for Effective Delivery of Camptothecin. *Polym. Chem.* **2012**, *3*, 1958–1961. DOI: 10.1039/c2py20201h.

[55] Gu, J.; Hao, J.; Fang, X.; Sha, X. Factors Influencing the Transfection Efficiency and Cellular Uptake Mechanisms of Pluronic P123-Modified Polypropyleneimine/pDNA Polyplexes in Multidrug Resistant Breast Cancer Cells. *Coll. Surf. B Biointerfaces* **2016**, *140*, 83–93. DOI: 10.1016/j.colsurfb.2015.12.023.

[56] Saxena, V.; Hussain, D. Formulation and in Vitro Evaluation of 17-Allyamino-17-Demethoxygeldanamycin (17-AAG) Loaded Polymeric Mixed Micelles for Glioblastoma Multiforme. *Coll. Surf. B Biointerfaces* **2013**, *112*, 350–355. DOI: 10.1016/j.colsurfb.2013.07.031.